Rotor Position Detection Scheme for Synchronous Reluctance Motor Based on Current Measurements

Takayoshi Matsuo, *Member, IEEE*, and Thomas A. Lipo, *Fellow, IEEE*

***Abstract*—A rotor position detection scheme which utilizes the characteristics of the synchronous reluctance motor is proposed. In particular, the dependence of the self and mutual inductances on the rotor position is utilized. The motor currents are controlled by a transistor inverter in the manner of hysteresis current control. The inverter switching creates ripples in the phase currents. The rate change of current in the ripples is then detected and converted to a rotor position signal. The proposed scheme is aimed to provide rotor position information particularly at low rotor speed, even at zero rotor speed. Numerical analysis of the rate change of the phase current of the synchronous reluctance motor is also discussed.**

I. Introduction

THE synchronous reluctance motor has recently attracted the efforts of a number of researchers [1] and is gaining favor as a possible alternative for ac drives. While the improved rotor designs [2], [3] have made synchronous reluctance motors competitive to induction motors in terms of power factor and efficiency, it has been demonstrated [4] that its control performance with a field oriented control scheme is as good as other high-performance ac drives. Rotor position sensing techniques without rotating shaft sensors have recently been addressed [5], [6], [8] in order to reduce the cost of the drive and simplify the system. One position sensing scheme [5] provides rotor position information at the zero crossings of the phase current, that is, only six rotor position samples per one electrical cycle of a three-phase motor. High control performance cannot be expected with this scheme, particularly at low rotor speed. Another position sensing scheme utilizing the stator phase voltage third harmonic [6] has also effectively six position samples per one electrical cycle and is not effective at low rotor speed because the scheme requires the induced third harmonic voltage. A sensorless closed-loop speed control scheme using voltage and current signals [8] is not effective for low rotor speed operating conditions.

It is the purpose of this paper to propose and examine a rotor position detection scheme for a synchronous reluctance motor which is based on current measurements. The self and mutual inductances of the motor depend on the rotor position and hence the rate change of current which is associated with the inverter switching depends on the rotor position. Thus the rotor position can be identified with a proper sensing technique of the time rate change of current. The proposed scheme is aimed to provide rotor position information particularly at low rotor speed, even at zero rotor speed.

Paper IPCSD 95–15, approved by the Industrial Drives Committee of the IEEE Industry Applications Society for presentation at the 1994 Industry Applications Society Annual Meeting, Denver, CO, October 2–7. Manuscript released for publication January 23, 1995.

T. Matsuo was with the Department of Electrical and Computer Engineering, University of Wisconsin, Madison, WI 53706 USA. He is now with the Department of Electrical and Computer Engineering, McMaster University, Hamilton, Ontario, L8S 4K1 Canada.

T. A. Lipo is with the Department of Electrical and Computer Engineering, University of Wisconsin, Madison, WI 53706 USA.

IEEE Log Number 9411427.

II. Voltage and Inductance Equations of a Synchronous Reluctance Motor

The three-phase voltage equations of the synchronous reluctance motor can be described by the equations given below [7] in the stationary reference frame.

$$v_{as} = r_s i_{as} + \frac{d\lambda_{as}}{dt} \tag{1}$$

$$v_{bs} = r_s i_{bs} + \frac{d\lambda_{bs}}{dt} \tag{2}$$

$$v_{cs} = r_s i_{cs} + \frac{d\lambda_{cs}}{dt} \tag{3}$$

where v_{as}, v_{bs}, and v_{cs} are the motor phase voltages, r_s is the stator winding resistance and $\lambda_{as}, \lambda_{bs}$, and λ_{cs} are the flux linkages of three phases. The flux linkages can be expressed as

$$\lambda_{as} = L_{as,as} i_{as} + L_{as,bs} i_{bs} + L_{as,cs} i_{cs} \tag{4}$$

$$\lambda_{bs} = L_{as,bs} i_{as} + L_{bs,bs} i_{bs} + L_{bs,cs} i_{cs} \tag{5}$$

$$\lambda_{cs} = L_{as,cs} i_{as} + L_{bs,cs} i_{bs} + L_{cs,cs} i_{cs}. \tag{6}$$

Neglecting higher order harmonics, each self and mutual inductance of the machine has a second harmonic component in addition to the constant component. The self and mutual inductances are

$$L_{as,as} = L_{ls} + L_{0s} - L_{2s} \cos 2\theta_r \tag{7}$$

$$L_{bs,bs} = L_{ls} + L_{0s} - L_{2s} \cos\left(2\theta_r + \frac{2\pi}{3}\right) \tag{8}$$

$$L_{cs,cs} = L_{ls} + L_{0s} - L_{2s} \cos\left(2\theta_r - \frac{2\pi}{3}\right) \tag{9}$$

$$L_{as,bs} = -\frac{1}{2} L_{0s} - L_{2s} \cos\left(2\theta_r - \frac{2\pi}{3}\right) \tag{10}$$

$$L_{bs,cs} = -\frac{1}{2} L_{0s} - L_{2s} \cos 2\theta_r \tag{11}$$

$$L_{as,cs} = -\frac{1}{2} L_{0s} - L_{2s} \cos\left(2\theta_r + \frac{2\pi}{3}\right) \tag{12}$$

where L_{ls} represents the leakage inductance of the phase and

$$L_{0s} = \mu_0 r l N_s^2 \left(\frac{\pi}{8}\right)\left(\frac{1}{g_{\min}} + \frac{1}{g_{\max}}\right) \tag{13}$$

0093–9994/95$04.00 © 1995 IEEE

$$L_{2s} = \mu_0 r l N_s^2 \left(\frac{\pi}{8}\right)\left(\frac{1}{g_{\min}} - \frac{1}{g_{\max}}\right) \tag{14}$$

where $g_{\min}$ represents the d-axis equivalent air gap and $g_{\max}$ represents the q-axis equivalent air gap and r, l, and N_s denote the rotor radius, the core length, and the number of turns in series per phase. The direct axis and quadrature axis magnetizing inductances L_{md} and L_{mq} are expressed as

$$L_{md} = \frac{3}{2}(L_{0s} + L_{2s}) \tag{15}$$

$$L_{mq} = \frac{3}{2}(L_{0s} - L_{2s}) \tag{16}$$

and then

$$L_{0s} = \frac{1}{3}(L_{md} + L_{mq}) \tag{17}$$

$$L_{2s} = \frac{1}{3}(L_{md} - L_{mq}). \tag{18}$$

Using (17) and (18) for (7)–(12) and replacing notations of $L_{as,as}, L_{bs,bs}, L_{cs,cs}, L_{as,bs}, L_{bs,cs}$, and $L_{as,cs}$ with L_{aa}, $L_{bb}, L_{cc}, L_{ab}, L_{bc}$, and L_{ac}, respectively

$$L_{aa} = L_{ls} + \frac{1}{3}L_{md}(1 - \cos 2\theta_r) + \frac{1}{3}L_{mq}(1 + \cos 2\theta_r) \tag{19}$$

$$L_{bb} = L_{ls} + \frac{1}{3}L_{md}\left(1 - \cos\left(2\theta_r + \frac{2\pi}{3}\right)\right) + \frac{1}{3}L_{mq}\left(1 + \cos\left(2\theta_r + \frac{2\pi}{3}\right)\right) \tag{20}$$

$$L_{cc} = L_{ls} + \frac{1}{3}L_{md}\left(1 - \cos\left(2\theta_r - \frac{2\pi}{3}\right)\right) + \frac{1}{3}L_{mq}\left(1 + \cos\left(2\theta_r - \frac{2\pi}{3}\right)\right) \tag{21}$$

$$L_{ab} = -\frac{1}{3}L_{md}\left(\frac{1}{2} - \cos 2\left(\theta_r - \frac{\pi}{3}\right)\right) - \frac{1}{3}L_{mq}\left(\frac{1}{2} - \cos 2\left(\theta_r - \frac{\pi}{3}\right)\right) \tag{22}$$

$$L_{bc} = -\frac{1}{3}L_{md}\left(\frac{1}{2} + \cos 2\theta_r\right) - \frac{1}{3}L_{mq}\left(\frac{1}{2} - \cos 2\theta_r\right) \tag{23}$$

$$L_{ac} = -\frac{1}{3}L_{md}\left(\frac{1}{2} + \cos\left(2\theta_r + \frac{2\pi}{3}\right)\right) - \frac{1}{3}L_{mq}\left(\frac{1}{2} - \cos\left(2\theta_r + \frac{2\pi}{3}\right)\right) \tag{24}$$

where θ_r is the rotor position in electrical angle. Self inductances L_{aa}, L_{bb}, and L_{cc} are plotted in Fig. 1, where the parameters of an experimental motor were used to calculate the self and mutual inductances. In this case, the leakage inductance L_{ls} is 0.0077 H, the d-axis magnetizing inductance is 0.095 H, and the q-axis magnetizing inductance is 0.0084 H. Mutual inductances L_{ab}, L_{bc}, and L_{ac} are plotted in Fig. 2. Figs. 1 and 2 illustrate the dependence of the self and mutual inductances of the synchronous reluctance motor on the rotor position.

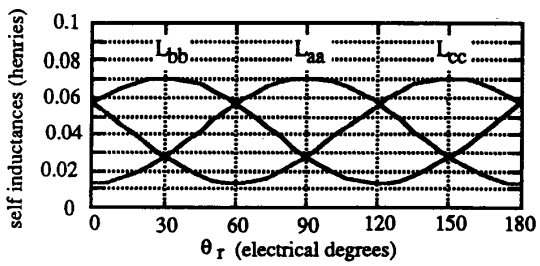

Fig. 1. Self inductances of a synchronous reluctance motor, L_{aa}, L_{bb}, and L_{cc} versus rotor position θ_r.

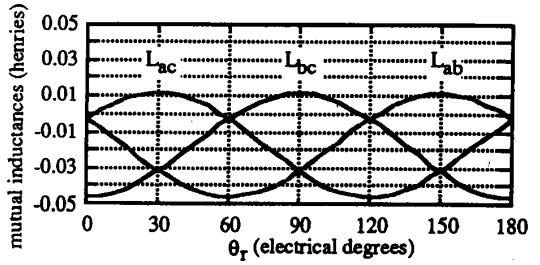

Fig. 2. Mutual inductances of a synchronous reluctance motor, L_{ab}, L_{bc}, and L_{ac} versus rotor position θ_r.

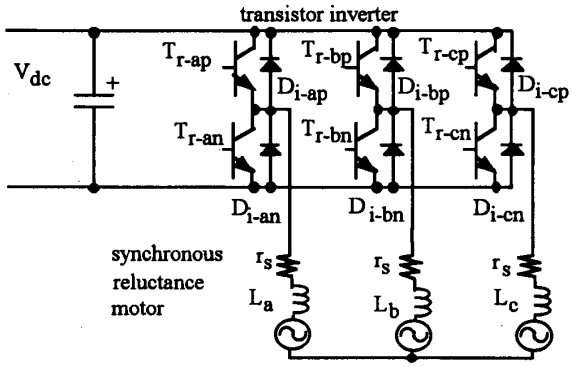

Fig. 3. A circuit diagram of a transistor inverter and a three phase synchronous reluctance motor with Y connected windings.

III. Rotor Position Detection Scheme Based on Current Measurements

A rotor position detection scheme has been developed based on the circuit diagram illustrated in Fig. 3. A conventional transistor inverter has been assumed to supply power to a synchronous reluctance motor and to therefore create current ripples which are essential for this rotor position detection scheme.

The synchronous reluctance motor has a special characteristic which is particularly good for rotor position detection, that is, the dependence of the self and mutual inductances on the rotor position, which are discussed and illustrated in the previous section. The self and mutual inductances of the motor

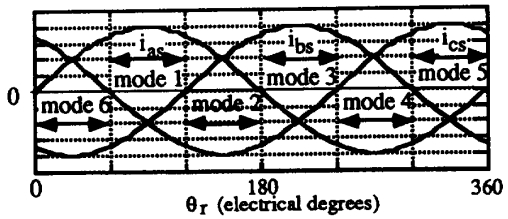

Fig. 4. Six conduction modes of a three phase transistor inverter based on the conducting directions of three phase currents.

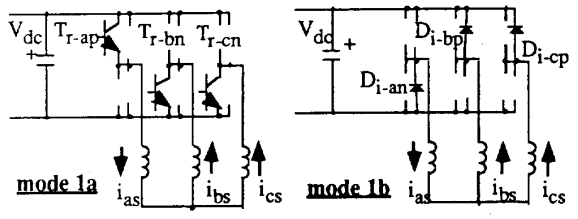

Fig. 5. Illustrated conduction modes, 1a and 1b of a three-phase transistor inverter based on the conducting directions of three-phase currents.

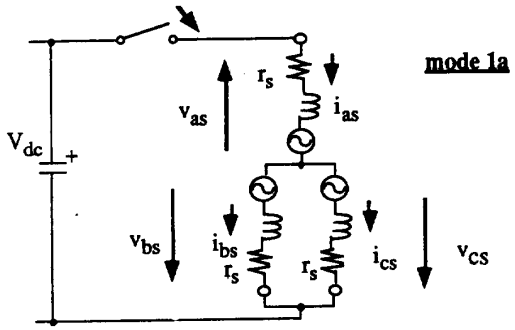

Fig. 6. The equivalent circuit for mode 1a, where the transistors $T_{r\text{-}ap}, T_{r\text{-}bn}$, and $T_{r\text{-}cn}$ are assumed to turn on at the same time.

depend on the rotor position and hence the rate change of current which is associated with the inverter switching depends on the rotor position. Thus the rotor position can be identified with a proper sensing technique of the rate change of current.

Fig. 4 shows six conduction modes of a three-phase transistor inverter based on the conducting directions of three-phase currents. Two different switching configurations are associated with each conduction mode, some of which are illustrated in Fig. 5. The conduction mode 1a is discussed first. Fig. 6 illustrates the equivalent circuit for mode 1a, where the transistors, $T_{r\text{-}ap}, T_{r\text{-}bn}$, and $T_{r\text{-}cn}$ are assumed to turn on at the same time. The constraints which are imposed to motor currents and voltages are given by the following equations:

$$V_{\rm dc} = v_{as} - v_{bs} \tag{25}$$

$$v_{bs} = v_{cs} \tag{26}$$

$$i_{as} = -(i_{bs} + i_{cs}). \tag{27}$$

To illustrate the rotor position detection scheme, (25)–(27) are solved for $i_{as}(t)$ by neglecting the stator resistance r_s and speed voltages. The solution of $i_{as}(t)$ including the stator resistance r_s and speed voltages is shown in a later section of this paper and the effect of the initial current and the rotor speed is discussed in detail. The following assumptions are made to simplify the equations and to visualize the characteristics of the rate change of current signals, which are to be utilized for rotor position decoding.

By substituting (1) and (2) into (25)

$$V_{\rm dc} = \frac{d\lambda_{as}}{dt} - \frac{d\lambda_{bs}}{dt} \tag{28}$$

and by using (4) and (5) for the expressions of λ_{as} and λ_{bs}

$$V_{\rm dc} = L_{aa}\frac{di_{as}}{dt} + L_{ab}\frac{di_{bs}}{dt} + L_{ac}\frac{di_{cs}}{dt} - \left(L_{ab}\frac{di_{as}}{dt} + L_{bb}\frac{di_{bs}}{dt} + L_{bc}\frac{di_{cs}}{dt}\right). \tag{29}$$

By substituting (2) and (3) into (26)

$$\frac{d\lambda_{bs}}{dt} = \frac{d\lambda_{cs}}{dt} \tag{30}$$

and by using (5) and (6) for the expressions of λ_{bs} and λ_{cs}

$$L_{ab}i_{as} + L_{bb}i_{bs} + L_{bc}i_{cs} = L_{ac}i_{as} + L_{bc}i_{bs} + L_{cc}i_{cs}. \tag{31}$$

The rate change of the phase a current di_{as}/dt can be solved from (27), (29), and (31).

$$\frac{di_{as}}{dt} = \frac{V_{\rm dc}}{L_{\rm mode\,1a}} \tag{32}$$

where

$$L_{\rm mode\,1a} = (L_{aa} - L_{ab} - L_{ac} + L_{bc}) + (-L_{ab} + L_{bb} + L_{ac} - L_{bc}) \cdot \frac{L_{ab} - L_{bc} - L_{ac} + L_{cc}}{L_{bb} - 2L_{bc} + L_{cc}}. \tag{33}$$

Equation (33) can be expressed in terms of L_{md} and L_{mq} by substituting (7)–(12) into (33), that is [see (34) at bottom of page].

$$L_{\rm mode\,1a} = L_{ls} + L_{md}\left(\frac{1}{2} - \cos 2\theta_r\right) + L_{mq}\left(\frac{1}{2} + \cos 2\theta_r\right) + \left(L_{ls} + L_{md}\left(\frac{1}{2} + \cos 2\left(\theta_r - \frac{\pi}{3}\right)\right) + L_{mq}\left(\frac{1}{2} - \cos 2\left(\theta_r - \frac{\pi}{3}\right)\right)\right) \cdot \frac{L_{ls} + L_{md}\left(\frac{1}{2} + \cos 2\left(\theta_r + \frac{\pi}{3}\right)\right) + L_{mq}\left(\frac{1}{2} - \cos 2\left(\theta_r + \frac{\pi}{3}\right)\right)}{2L_{ls} + L_{md} + L_{mq} + (L_{md} - L_{mq})\cos 2\theta_r}. \tag{34}$$

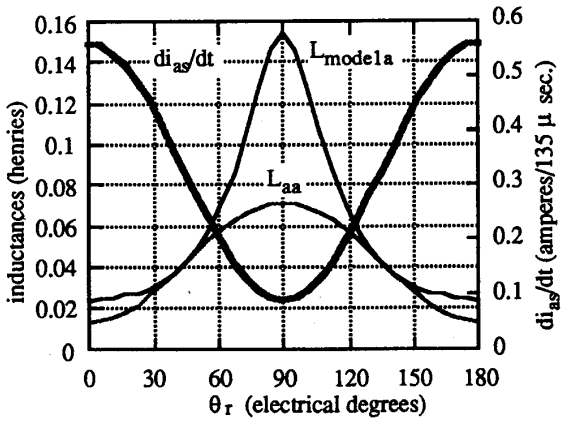

Fig. 7. The plotting of the rate change of the current di_{as}/dt, inductances L_{aa} and $L_{\text{mode 1a}}$ versus the rotor position θ_r.

Fig. 7 shows the plotting of the rate change of the current di_{as}/dt versus the rotor position θ_r by substituting the self and mutual inductances which are described in (7)–(12) into (33). The same motor parameters as for Figs. 1 and 2 are used for the calculations.

By an observation of the conduction modes of Fig. 5, it is clear that the equivalent circuit of Fig. 6 can be applied to the mode 4a. The same equivalent circuit with the reversed polarity of the dc bus voltage V_{dc} is applied to the modes 1b and 4b. The rate change of the phase b and c current, di_{bs}/dt and di_{cs}/dt, are also given by (35) and (37), that is

$$\frac{di_{bs}}{dt} = \frac{V_{\text{dc}}}{L_{\text{mode 3a}}} \tag{35}$$

where

$$\begin{aligned} L_{\text{mode 3a}} = &(L_{bb} - L_{ab} - L_{bc} + L_{ac}) \\ &+ (-L_{ab} + L_{aa} + L_{bc} - L_{ac}) \\ &\cdot \frac{L_{ab} - L_{ac} - L_{bc} + L_{cc}}{L_{aa} - 2L_{ac} + L_{cc}} \end{aligned} \tag{36}$$

$$\frac{di_{cs}}{dt} = \frac{V_{\text{dc}}}{L_{\text{mode 5a}}} \tag{37}$$

where

$$\begin{aligned} L_{\text{mode 5a}} = &(L_{cc} - L_{bc} - L_{ac} + L_{ab}) \\ &+ (-L_{bc} + L_{bb} + L_{ac} - L_{ab}) \\ &\cdot \frac{L_{bc} - L_{ab} - L_{ac} + L_{aa}}{L_{bb} - 2L_{ab} + L_{aa}}. \end{aligned} \tag{38}$$

Fig. 8 shows three curves of the rate change of the phase currents which can be utilized to convert to a rotor position signal. It is apparent that three independent signals are available at every rotor position for the purpose of identifying the rotor position.

Fig. 9 illustrates the sensing scheme of the rate change of current. The motor phase currents are controlled in the manner of hysteresis current control. The current is controlled to follow the current reference with current ripples within the current bandwidth by means of the inverter switching. The

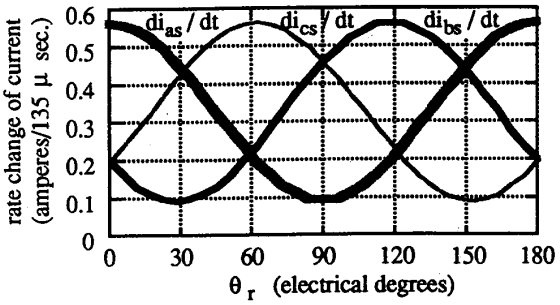

Fig. 8. Three curves of the rate change of the current di_{as}/dt, di_{bs}/dt, and di_{cs}/dt versus the rotor position θ_r.

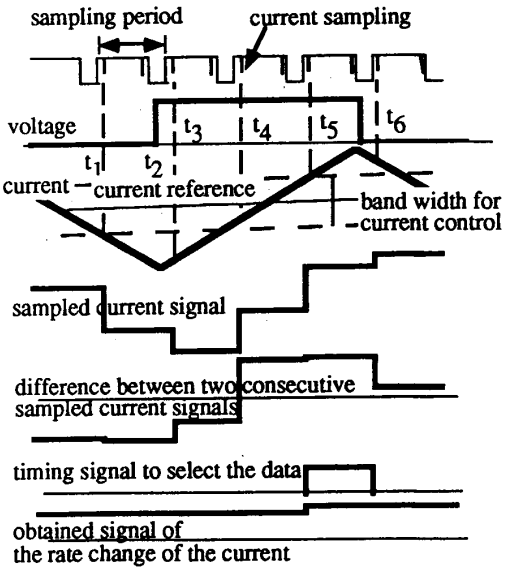

Fig. 9. Illustration of the sensing scheme of the rate change of current.

sampled current signal at t_1 in Fig. 9 is below the desired value and then switching devices are triggered to apply a positive voltage to the corresponding windings. The current starts increasing at t_2 and keeps increasing until the sampled current exceeds the upper level of the desired current band and then the switching condition is changed at t_6 to decrease the current. The rate change of current is calculated as the difference of the consecutive two sampled current signals. A timing signal is implemented to identify the correct sample timing and pick up the correct rate change of current signal.

The frequency of the current ripple thus varies as the rate change of current changes, and depends on the setting of the current bandwidth. For the experimental system, the rate change of current varies from 0.1–0.5 A per 135 μs and the current band width is set at 0.94 A which is about 18% of the peak value of the phase current. It takes about two to three samples at the highest rate change of the current and about nine to ten samples at the lowest rate change of the current to increase the current from the bottom to the top of the ripple.

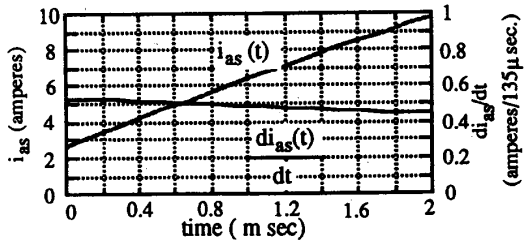

Fig. 10. Plot of the phase current $i_{as}(t)$ and the rate change of current $di_{as}(t)/dt$ for the initial conditions of the phase current $i_{as}(0) = 2.6$ A and the rotor speed $\omega_r = 0.0$ rad/s at the rotor position $\theta_r = 0.0$ rad.

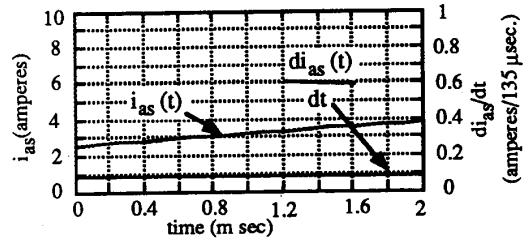

Fig. 11. Plot of the phase current $i_{as}(t)$ and the rate change of current $di_{as}(t)/dt$ for the initial conditions of the phase current $i_{as}(0) = 2.6$ A and the rotor speed $\omega_r = 0.0$ rad/s (a) at the rotor position $\theta_r = 0.0$ rad, and (b) at the rotor position $\theta_r = \pi/2$ rad.

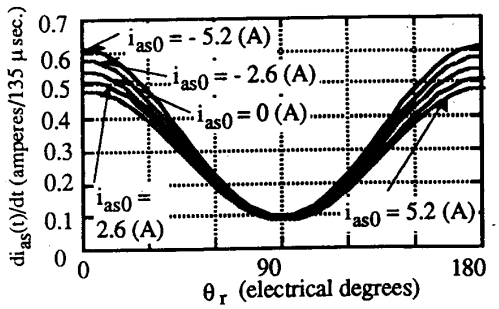

Fig. 12. Plot of the rate change of the current $di_{as}(t)/dt$ versus the rotor position θ_r for different initial conditions of the phase current, that is, $i_{as0} = 0.0, 2.6, 5.2, -2.6$, and -5.2 A and the rotor speed $\omega_r = 0.0$ rad/s.

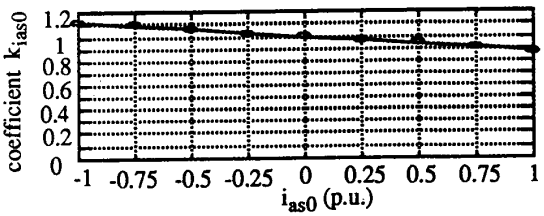

Fig. 13. The calculation result of the coefficient k_{ias0} versus the initial current i_{as0}.

IV. Analysis of the Rate Change of Current

The solution for the phase a current, $i_{as}(t)$, after the switch is closed in Fig. 6 is given by (39).

$$i_{as}(t) = \frac{V_{\rm dc}}{L_{\rm mode\,1a}}(c_1 + c_2 e^{-at} + c_3 e^{-bt}) \qquad (39)$$

where a, b, c_1, c_2, and c_3 are functions of inductances, L_{md}, L_{mq}, and L_{1s}, rotor position, θ_r, rotor speed, ω_r, and initial stator currents.

The dependence of the behavior of the phase a current, $i_{as}(t)$, on initial conditions such as rotor speed and initial current can be analyzed numerically by using (39). An example of the phase current trace after the switches are closed for the conduction mode 1a is shown in Figs. 10 and 11, where the phase current $i_{as}(t)$ and the rate change of current $di_{as}(t)/dt$ are plotted for the initial conditions of the phase current $i_{as}(0) = 2.6$ A and the rotor speed $\omega_r = 0.0$ rad/s at the rotor position $\theta_r = 0.0$ rad and $\theta_r = \pi/2$ rad. The motor parameters used in this analysis are the ones of the experimental synchronous reluctance motor, that is, the stator resistance $r_s = 1.58\ \Omega$, the leakage inductance $L_{1s} = 0.0077$ H, the d-axis magnetizing inductance $L_{md} = 0.095$ H, the q-axis magnetizing inductance $L_{mq} = 0.0084$ H, the rated phase current $i_{as\text{-rated}} = 3.7$ A in rms and the rated rotor speed $\omega_r = 272.3$ rad/s in electrical angular speed, that is, 1300 r/min.

The rate change of current $di_{as}(t)/dt$ versus the rotor position θ_r is plotted in Fig. 12 for different initial conditions of the phase current. That is, $i_{as0} = 0.0$, 2.6, 5.2, -2.6, and -5.2 A, which correspond to 0, 0.5, 1.0, -0.5, and -1.0 per unit of the peak value of the rated phase current, where the rotor speed $\omega_r = 0.0$ rad/s. The rate change of current decreases by 12% for an increase of the initial current from zero to 1.0 p.u. and increases 12% for a decrease of the initial current from zero to -1.0 p.u.

The rate change of the current is calculated as the difference of the two sampled currents $i_{as}(t = 540\,\mu\text{s})$ and $i_{as}(t = 405\,\mu\text{s})$. The ratio of the rate change of the current for the initial current i_{as0} of 0.0 A to one for 2.6 A is independent of the rotor position and is about 0.94 and 0.88 for the initial current i_{as0} of 0.0 A to one for 5.2 A. Fig. 13 is the plot of the calculation result of the coefficient k_{ias0} versus the initial current i_{as0}, which is the ratio of the rate change of the current di_{as}/dt under the condition of the specific initial current to the rate change of current for zero initial current. The coefficient k_{ias0} is set at 1.0 for the case where the initial current is zero. Fig. 14 shows the calculation result of the rate change of the current, di_{as}/dt, versus the rotor position θ_r for different rotor speeds, where the initial current is 0.0 p.u.. A rotor speed of 0.1 p.u. contributes to about a 2.7% increase of the rate change of current when the initial current is zero, while a rotor speed of -0.1 p.u. contributes to about a 2.7% decrease.

Fig. 15 shows the calculation result for the rate change of the current, di_{as}/dt, versus the rotor position θ_r for different rotor speeds, where the initial current is 0.5 p.u. With the existence of the initial conditions of rotor speed and initial current, the curve of the rate change of current versus rotor position shifts left or right by a certain angle. The curve shifts left when the polarity of $\omega_r * i_{as0}$ is positive and shifts right when the polarity is negative.

Fig. 16 shows the calculation for the phase shift of the rotor position decoding curve versus rotor speed ω_r, where the initial current is 0.5 p.u. The amount of angle shift depends on the rate change of current value which is used to be converted

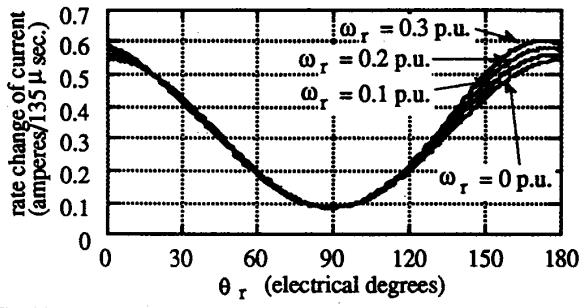

Fig. 14. The calculation result of the rate change of the current di_{as}/dt versus rotor position θ_r for different rotor speeds, where the initial current is 0.0 p.u.

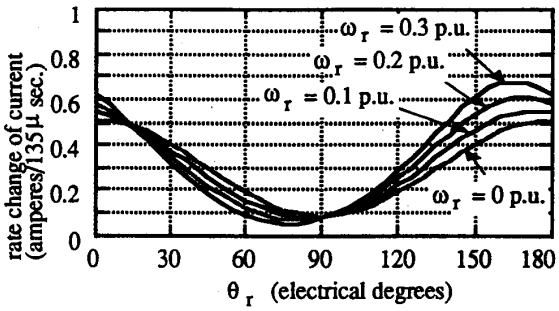

Fig. 15. The calculation result of the rate change of the current di_{as}/dt versus rotor position θ_r for different rotor speeds, where the initial current is 0.5 p.u.

to a rotor position signal and about six electrical degrees for $di/dt = 0.2$ A/135 μs, the rotor speed of 0.1 p.u., and the initial current of 0.5 p.u. Fig. 17 shows the calculation result of the rate change of the current di_{as}/dt versus rotor position θ_r for different rotor speeds and initial current. Compensation can be made to the curves in Fig. 17 to correct the phase shift due to rotor speed and initial current, based on the analysis result in this section. The applied simple rule of compensation is, first, to correct the amplitude of the rate change of current by the factor of 1.13 for the initial current of plus one per unit and by the factor of 0.89 for the initial current of minus one per unit. The second rule is to correct the amplitude of the rate change of current by the factor of 0.97 for a rotor speed of 0.1 per unit and by the factor of 1.027 for a rotor speed of -0.1 per unit. The third rule is to shift the curve right ten electrical degrees for a rotor speed of 0.1 per unit and an initial current of one per unit. Fig. 18 shows the calculation result of the corrected curves of the rate change of current versus rotor position. It is thus demonstrated that a simple compensation scheme can improve accuracy of the rotor position detection.

V. Block Diagram for Implementing Proposed Rotor Position Detection Scheme

Fig. 19 shows the overall control strategy for a synchronous reluctance motor where the absolute encoder is replaced with the proposed rotor position detection scheme. The rotor position detector converts the measured stator current signals into

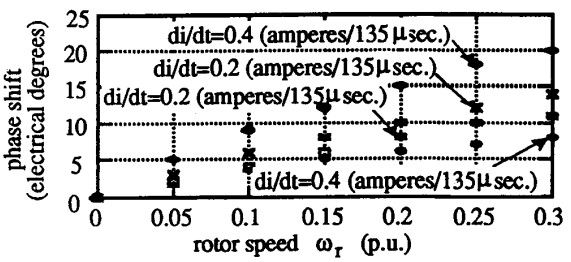

Fig. 16. The calculation result of the phase shift of the rotor position decoding curve versus rotor speed ω_r, where the initial current is 0.5 p.u.

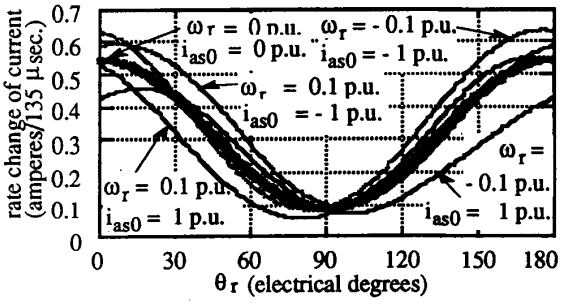

Fig. 17. The calculation result of the rate change of the current di_{as}/dt versus rotor position θ_r for different rotor speeds and initial currents.

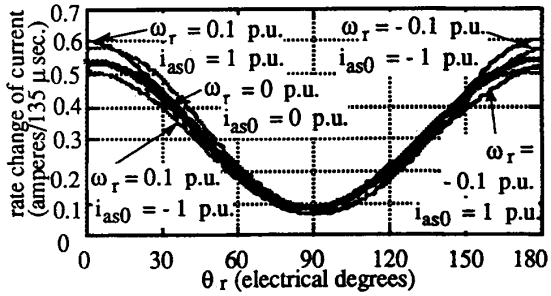

Fig. 18. The calculation result of the corrected curves of the rate change of current di_{as}/dt versus rotor position using a simple compensation scheme.

a rotor position signal and then the sine and cosine of the angular position of the rotor is established. These sinusoidal components are used to refer the command stator currents from the rotating (d–q) axes to the physical (stationary) reference frame.

The three-phase current controller provides a switching command to each transistor of the inverter to have each phase current follow the stator current command in the manner of hysteresis current control. The inverter switching generates ripples in the stator current and the rate change of current is measured and converted to a rotor position signal. By implementing the current controller with software, the controller possesses all the information on the inverter switching status. The controller includes a table of the rotor position versus three-phase rate change of current, which is prepared with the measured data for a specific motor. The rate change of current is calculated for each phase and the obtained signals

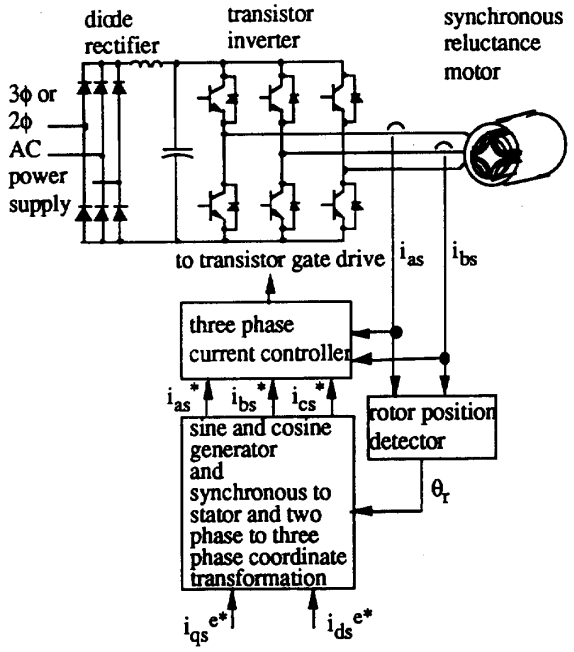

Fig. 19. A control configuration for a synchronous reluctance motor drive with a rotor position detection scheme based on current measurements.

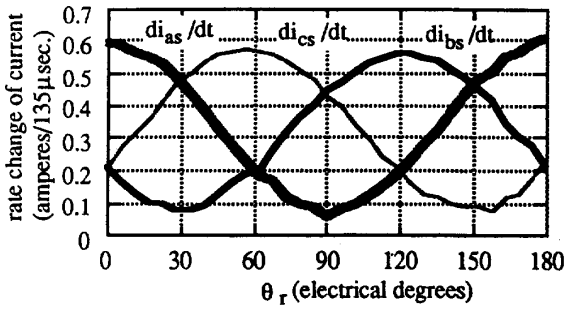

Fig. 20. Experimental results of the rate change of current versus rotor position θ_r for three phases.

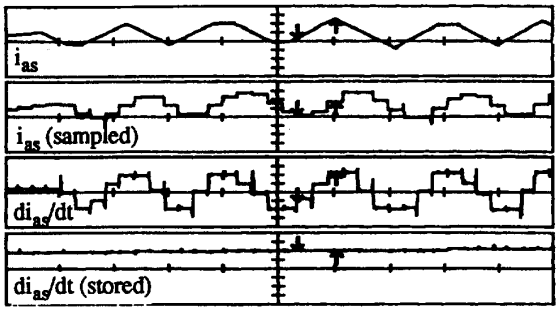

Fig. 21. Experimental results of the rotor position detection scheme. From top to bottom: (i) the phase a current i_{as} (0.5 A/div), (ii) the sampled phase a current signal (0.4 A/div), (iii) the rate change of current signal (0.2 A/135 μs/div), and (iv) the rate change of current signal stored in the controller (0.2 A/135 μs/div). The time scale is 0.5 μs/div.

are converted to a rotor position signal by using the table. The rate change of current for a specific phase is only refreshed at the sampling timing corresponding to a specific conduction mode.

VI. Experimental Results

The rotor position detection scheme for a synchronous reluctance motor has been completely implemented in the laboratory in order to verify and study the proposed scheme. All the control functions are implemented with software in a digital signal processor and a conventional transistor inverter was used to drive the motor where the dc bus voltage of the inverter was 100 V. The experimental synchronous reluctance motor was used, which has a saliency ratio L_{ds}/L_{qs} of 6.7 for the unsaturated conditions and 6.4 for the saturated conditions, and almost no cross coupling effects on both d- and q-axes magnetizing inductances.

Fig. 20 shows the experimental results of the rate change of current versus rotor position θ_r for three phases where the rate change of current data were sampled while the motor was locked at each specified rotor position. These three curves are utilized to convert the rate change of current signal to a rotor position signal.

Fig. 21 shows an experimental result of the rotor position detection scheme where the related waveforms of the phase a current i_{as}, the sampled phase a current signal and the rate change of current signal, and the rate change of current signal stored in the controller are shown. The d-axis current command i_{ds}^* is 1.1 A and the q-axis current command i_{qs}^* is 0.47 A. The sampling period of the controller is 135 μs and the sampling timing is clearly shown in Fig. 21. The plotted waveforms of the phase current and the rate change of current are output signals from digital to analog converters and are delayed for one sampling period. The rate change of a current signal is the difference of two consecutive sampled current signals.

Converted from the rate change of current data, the rotor position signal has a frequency of twice the rotor electrical frequency. This is because the rate change of current is a function of the motor impedances and thus does not have information on the polarities of poles. The calculated position signal $2\theta_r$ must be converted to the position signal θ_r. The signal $2\theta_r$ takes an electrical angle between 0 and π. The controller must continue to keep tracking the position signal $2\theta_r$ in order to create θ_r signal by adding π to the $2\theta_r$ signal every other half electrical cycle.

Figs. 22 and 23 show the waveforms of the rotor position signals $2\theta_r$ and θ_r with the absolute encoder signal θ_r and three-phase currents while the motor starts from rest and accelerates forward with increasing rotor speed up to about 130 r/min. Fig. 24 shows the waveforms of the same quantities in Fig. 22 while the motor reverses its rotational direction from forward to reverse. The d-axis current command i_{ds}^* is 1.1 A and the q-axis current command i_{qs}^* is −0.62 A.

It should be noted that the proposed rotor position detection scheme is most effective at low rotor speed including zero shaft speed. Comparison between the rotor position signal which is

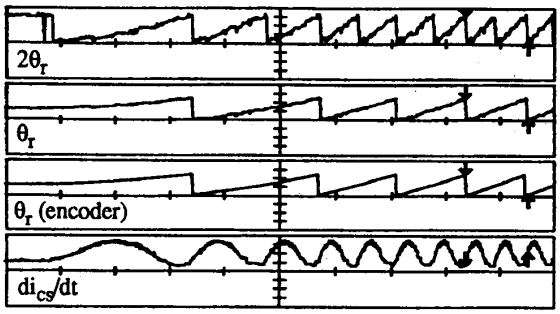

Fig. 22. Experimental results of the rotor position detection scheme for starting the motor in the forward direction. From top to bottom: (i) the rotor position signal $2\theta_r$ (0.2 V/div), (ii) the rotor position signal θ_r calculated by the rotor position detection scheme (0.5 V/div), (iii) the rotor position signal θ_r by the encoder (0.5 V/div), and (iv) di_{cs}/dt data stored in the controller (0.2 A/135 μs/div). The time scale is 2 s/div.

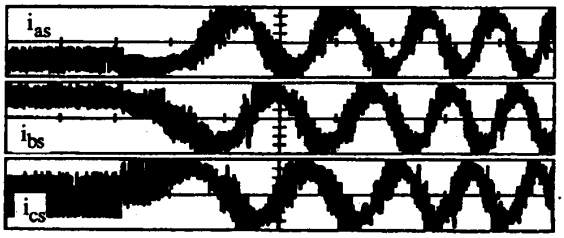

Fig. 23. Experimental results of the rotor position detection scheme. From top to bottom: (i) the phase a current i_{as} (0.4 A/div), (ii) the phase b current i_{bs} (0.4 A/div), and (iii) the phase c current i_{cs} (0.4 A/div). The time scale is 2 s/div.

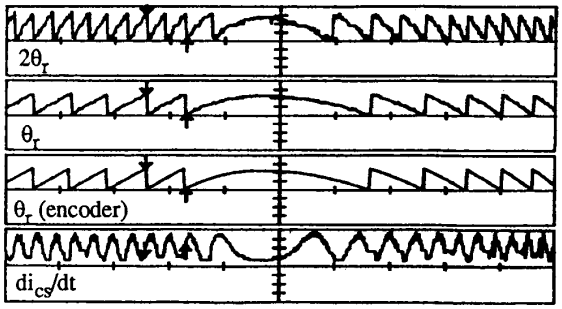

Fig. 24. Experimental results of the rotor position detection scheme for changing the rotational direction from forward to reverse. From top to bottom: (i) the rotor position signal $2\theta_r$ (0.2 V/div), (ii) the rotor position signal θ_r calculated by the rotor position detection scheme (0.5 V/div), (iii) the rotor position signal θ_r by the encoder (0.5 V/div), and (iv) di_{cs}/dt data stored in the controller (0.2 A/135 μs/div). The time scale is 2 s/div.

detected with the proposed scheme and the monitored rotor position signal by means of an absolute encoder shows that the synchronous reluctance motor can start smoothly from rest and is very well controlled without an absolute rotor position sensor. It is demonstrated that the motor torque is adequately controlled and that the control scheme is stable.

The accuracy of the rotor position detection however, deteriorates as the motor speed increases, as discussed in the previous section. However, the argument suggests that there exists means to compensate the error components associated with rotor speed and initial current terms. Numerical analysis, however, indicates that a complex three-dimensional table which is a function of rotor speed and initial current may be necessary to compensate the rotor position signal above 10% of the rated speed for the experimental synchronous reluctance motor in order to keep the position error within 10 electrical degrees. However, this does not pose a serious limitation since the motor can be readily controlled beyond this speed by integrating the voltage behind the stator iR drop to synthesize the stator flux linkages [8].

The resolution of the detected rotor position signal depends upon the resolution of the current measurements and the current sampling, that is, on the resolution of the digital to analog converter in the control system. The resolution of the detected rotor position signal is also related to the controller sampling time and the current control bandwidth.

The minimum value of the rate change of current data is 6 and the maximum is 63 in the controller. The resolution of the rotor position signal is 90/57 = 1.6 electrical degrees for the experimental system which uses 12-b A/D converter. The resolution can be increased by increasing the number of bits of A/D converters or increasing the sampling time. The amplitude of ripple currents is, however, increased if the sampling time is increased. The sampling time of the controller is 135 μs and the current control band width is 0.94 A for the experimental drive system. A specific current ripple is required to detect the rate change of current. The expected maximum rate change of current is about 0.6 A/135 μs and thus the current control band width should be larger than 0.6 A.

A combination of the proposed scheme and another rotor position detection scheme which is effective for high rotor speed, for example, utilization of the motor voltages, may offer a good rotor position detection scheme to cover all possible motor speed conditions.

VII. Conclusion

A rotor position detection scheme for synchronous reluctance motors which is based on current measurements has been proposed and examined in this paper. The proposed rotor position detection scheme utilizes the dependence of the self and mutual inductances of the synchronous reluctance motor on the rotor position. The rate change of current in the ripples is detected and converted to a rotor position signal. The proposed scheme can provide rotor position information particularly at low rotor speed, even at zero speed. Good control performance has been obtained at low rotor speed, which indicates that the proposed rotor detection scheme can be applied to a position sensorless control scheme for a synchronous reluctance motor combined with other rotor position detection schemes which are effective for high rotor speed.

References

[1] T. A. Lipo, "Synchronous reluctance machines—A viable alternative for ac drives?" *Electric Machines and Power Syst.*, vol. 19, pp. 659–671, 1991.

[2] T. Matsuo and T. A. Lipo, "Rotor design optimization of synchronous reluctance machine," *IEEE Trans. Energy Conversion*, vol. 9, no. 2, pp. 359–365, June 1994.
[3] D. A. Staton, T. J. E. Miller, and S. E. Wood, "Optimization of the synchronous reluctance motor geometry," in *Conf. Rec. Electrical Machines and Drives*, London, UK, 1991, pp. 156–160.
[4] T. Matsuo and T. A. Lipo, "Field oriented control of synchronous reluctance machine," in *Conf. Rec. IEEE Power Electron. Specialists Conf.*, June 1993, pp. 425–431.
[5] M. S. Arefeen, M. Ehsani, and T. A. Lipo, "An analysis of the accuracy of indirect shaft sensor for synchronous reluctance motor," in *Conf. Rec. IEEE Ind. Applicat. Soc. Annu. Meeting*, Oct. 1993, pp. 695–700.
[6] L. Kreindler, A. Testa, and T. A. Lipo, "Position sensorless synchronous reluctance motor drive using the stator phase voltage third harmonic," in *Conf. Rec. IEEE Ind. Applicat. Soc. Annu. Meeting*, Oct. 1993, pp. 679–686.
[7] T. A. Lipo and D. W. Novotny, "Dynamics and control of ac drives," ECE 711 Course Notes, Department of Electrical and Computer Engineering, Univ. of Wisconsin, Madison, 1991.
[8] R. Lagerquist, I. Boldea, and T. J. E. Miller, "Sensorless control of the synchronous reluctance motor," *IEEE Trans. Ind. Applicat.*, vol. 30, pp. 673–682, May/June 1994.

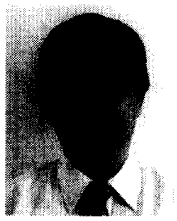

Takayoshi Matsuo (S'90–M'94) was born in Himeji, Japan. He received the B.E. degree in electrical engineering and the M.E. degree in applied electronics from the Tokyo Institute of Technology, Japan, in 1975 and 1977, respectively, and the M.S. and Ph.D. degrees in electrical engineering from the University of Wisconsin, Madison, in 1983 and 1994, respectively.

From 1977 to 1989, he was an electrical engineer in the Power Electronics Department, Mitsubishi Electric Corporation, Japan. He was a research associate in the Department of Electrical and Computer Engineering, University of Wisconsin, Madison, in 1994. He is currently a postdoctoral fellow at McMaster University, Hamilton, Ontario, Canada. His research interests are in ac drives, power electronics, and electrical machines.

Thomas A. Lipo (M'64–SM'71–F'87), for photograph and biography, please see p. 859 of this TRANSACTIONS.